BINDING OF PENTACHLOROIRIDITE TO PLASMA POLYMERIZED VINYLPYRIDINE FILMS AND ELECTROCATALYTIC OXIDATION OF ASCORBIC ACID

J. Facci and Royce W. Murray
Kenan Laboratories of Chemistry
University of North Carolina
Chapel Hill, N.C. 27514

ABSTRACT

Coordination of $[IrCl_5(acetonato)]^{2-}$ in acetone/methylene chloride to a film of vinylpyridine RF plasma polymerized on a carbon electrode results in an electrode surface wave at +0.40 volt *vs.* S.C.E. in 1 *M* H_2SO_4 . This potential is more negative than expected for $-PyIrCl_5^{2-}$ coordination. Charge transport in the film is very fast and the film catalyzes the oxidation of ascorbic acid at a diffusion controlled rate. The film electrochemistry is sensitive to the choice of supporting electrolyte cation but not anion.

BINDING OF PENTACHLOROIRIDITE TO PLASMA POLYMERIZED VINYLPYRIDINE FILMS AND ELECTROCATALYTIC OXIDATION OF ASCORBIC ACID

J. Facci and Royce W. Murray
Kenan Laboratories of Chemistry
University of North Carolina
Chapel Hill, N.C. 27514

BRIEF

Electrochemistry and electrocatalytic reactivity of carbon electrodes coated with films of pentachloroiridite-metallated plasma polymerized vinylpyridine are described.

Investigations of electron transfer-mediated electrocatalytic reactions evoked by electrodes coated with molecularly designed redox-active films have been of considerable recent interest (1-11). Efforts have been directed at theoretical and quantitative kinetic descriptions of such reactions (9, 12-16). The electrocatalysis described here grew out of our investigations of electrodes coated using RF plasma polymerization reactions (15,17,18) and our interest in binding iridium complexes to electrode surfaces (19). Vinylferrocene, for instance, can be plasma polymerized to form stable films with expectable ferrocene-ferricenium electrochemical reactivity (15,17,18). Having used the solvento complex $[IrCl_5(acetonato)]^{2-}$ for coordination reactions to pyridine and to vinylpyridine monomers, a natural extension was the use of plasma polymerization to prepare "polyvinylpyridine" films from vinylpyridine and the reaction of the solvento iridium complex with this film (in a manner akin to that of Oyama and Anson (20)). As described here the plasma film chemistry proves to be not simply that of pyridine and the ligand site binding the iridium is unknown. The iridium metallated film is, however, exceptionally stable and also catalyzes the oxidation of ascorbic acid at a diffusion controlled rate.

EXPERIMENTAL

Electrodes. Teflon shrouded glassy carbon disk electrodes (0.071 cm^2) were constructed as described elsewhere (21) except that conductive silver epoxy was used to seal the glassy carbon rod (Atomergic) concentrically within the brass holder, and the heat shrunk Teflon shroud was made concentric with the brass holder by gentle lathing. Electrodes were mirror polished with 1 μm diamond paste (Buehler) and washed with distilled water prior to use.

Equipment. Cyclic voltammetry was done with a PAR Model 175 Signal Generator

and a locally designed potentiostat, rotated disk voltammetry with a PIR Rotator (Pine Instrument Co., Grove City, PA), and potential step chronoamperometry with a PAR Model 173 Potentiostat/Galvanostat in conjunction with a Tektronix oscilloscope. Except for rotated disk experiments which were done in a 50 ml beaker under N_2, electrochemical experiments were performed in a small volume (1.5 ml) three electrode cell with Pt auxiliary electrode and Luggin probe connection to a sodium chloride saturated calomel electrode (SSCE).

Plasma polymerization was effected with a Harrick Scientific (Ossining, N.Y.) inductively coupled RF plasma unit (17).

Chemicals. $LiClO_4$, $NaClO_4$, $CsClO_4$ (G. Frederick Smith), tetraethylammonium chloride (Et_4NCl, Eastman), tetra-n-butylammonium bromide (Bu_4NBr, MCB) and KCl (Fisher) supporting electrolytes and 3-hydroxytyramine hydrochloride (dopamine, Aldrich) and L-ascorbic acid were used as received. D-(-)-epinephrine (Eastman), used as received, was stored in a freezer. 4-vinylpyridine (Aldrich) was purified by passing over neutral alumina (Fisher, Brockman Activity 1) and stored in a freezer.

Polymer Films. Plasma polymerized 4-vinylpyridine (PPVPy) films were deposited on glassy carbon electrodes as follows. The plasma chamber was cleaned prior to each deposition by successive rinses with dimethylsulfoxide, water and acetone and followed by pumping of the chamber to 60 mtorr and igniting the Ar plasma (lowest radiofrequency power setting, $\sim$ 10 watts) for 20 minutes under a 200 millitorr argon leak. A brief exposure of the chamber to the atmosphere occurs next, during placement of the electrodes in the chamber. Since prior work with vinylferrocene had revealed substantial sensitivity of the plasma reaction to reactor geometry (17), the carbon electrodes were reproducibly positioned in wells number 1, 2, and 3 of a glass flute (Figure 1) placed at a marked position on the central axis of the cylindrical

plasma chamber. The chamber was alternately evacuated and flushed with Ar at 1 torr, then 10-20 μl of purified 4-vinylpyridine was quickly added to well number 4 (closest to the chamber gas inlet). Following a further 30 second Ar flush at 1 torr, the plasma was ignited (∿ 10 watts) under 350 mtorr Ar for 180 seconds, after which the electrodes were removed. Shorter plasma reaction times gave films which dissolved in dichloromethane and acetone.

The plasma polymerized vinylpyridine (PPVPy) films were visibly colored. This is apparently an interference effect. Electrodes in well 1 tended to be deep red to orange, those in well 2, yellowish, while those in well 3, just inside the plasma, were blue to deep purple. Electrodes at positions beyond well 1 were rust colored and these films were apparently too thick for electrochemical study. The quantity of PPVPy present was such that it was scrapeable in palpable amounts and this was subjected to elemental analysis, indictating an empirical formula of $C_7H_{8.3}N_1O_{1.8}$. Only those electrodes which were visibly colored as in wells 1-3 were found to be electrochemically useful. PPVPy coatings prepared on platinum electrodes were not colored and dissolved in dichloromethane and acetone, solvents used for the introduction of $-IrCl_5^{2-}$ groups.

Metallation of Polymer. Pentachloroiridite centers were introduced into the plasma polymerized vinylpyridine films by modifying the procedure of Bottomley (22). Sodium nitrosylpentachloroiridite(III), $NaIrCl_5(NO)$, synthesized by a literature preparation (22), was precipitated from concentrated HCl by the addition of tetraphenylarsonium chloride ($AsPh_4Cl$). This golden brown solid is soluble in CH_2Cl_2 (red-brown solution). Tetraphenylarsonium azide was prepared by precipitation from a mixture of $AsPh_4Cl$ and NaN_3 aqueous solutions, collected and dried in vacuo.

A glassy carbon electrode coated with PPVPy was contacted with a N_2 degassed 75% CH_2Cl_2/25% acetone solution of $AsPh_4IrCl_5(NO)$ in a serum capped vial under subdued light to which was added, via syringe, a stoichiometric quantity of $AsPh_4N_3$ in N_2 degassed 75% CH_2Cl_2/25% acetone. The mixture immediately turned deep green indicative of the acetonato complex, $IrCl_5(acetone)^{2-}$. The acetone of the solvent complex is easily displaced by strong π-acid ligands present in the plasma polymer film resulting in a pendant $IrCl_5^{2-}$ moiety. The Ir modified electrode, designated C/PPVPy - $IrCl_5^{2-}$, was rinsed with methanol and water and air dried prior to use. The overall reaction scheme is

$$AsPh_4IrCl_5(NO) + AsPh_4N_3 \xrightarrow{CH_2Cl_2} (AsPh_4)_2IrCl_5(N_2O) + N_2\uparrow \qquad (1)$$

$$(AsPh_4)_2IrCl_5(N_2O) + CH_3(CO)CH_3 \xrightarrow{CH_2Cl_2} (AsPh_4)_2IrCl_5(acetone) + N_2O\uparrow \qquad (2)$$

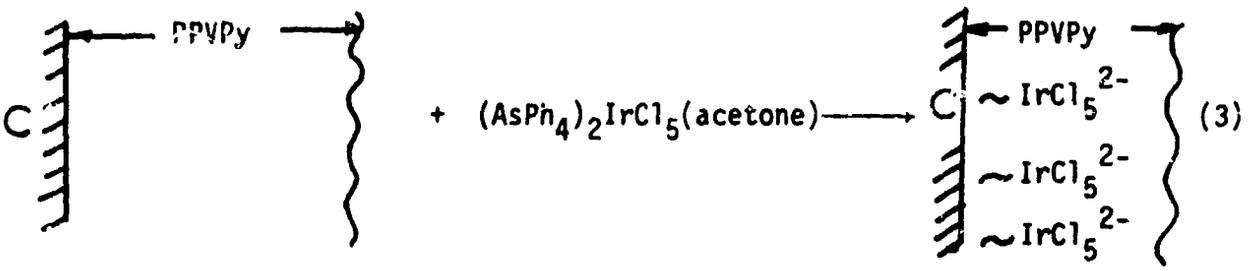

(3)

RESULTS AND DISCUSSION

Electrochemical Reactions of C/PPVPy ~ $IrCl_5^{2-}$ Films. In aqueous 1 M H_2SO_4 , unmetallated plasma polymerized vinylpyridine films exhibit cyclic voltammograms which, between 0 and +1.0 volt vs. S.C.E., demonstrate large but otherwise featureless background currents. The large background currents suggest that the microscopic surface area is quite large ; nevertheless the film surface has a glossy, reflecting appearance.

Reaction of PPVPy with $IrCl_5(CH_3COCH_3)^{2-}$, Rxn. 3, results in C/PPVPy ~ $IrCl_5^{2-}$ voltammograms in 1 M H_2SO_4 which display (Figure 2) a somewhat broad (typical E_{FWHM} ~ 240 mv.) wave at $E^{\circ\prime}_{surf}$ = +0.40 volt vs. S.C.E. The charges under the oxidation and reduction peaks are equal and correspond in this sample to a coverage of electroactive sites of 5.7×10^{-9} mol./cm.^{2} of geometric area, assuming n = 1. This electrochemical surface wave is remarkably stable. Cycling the electrode potential between 0 and +1.0 volt vs. S.C.E. for 1.5 days (12 hours at 200 mv./s. and 24 hours at 10 v./s.) in 1 M H_2SO_4 caused the peak currents at +0.40 volts to decrease by less than 3%. During these potential scans the electrode spent the equivalent of 18 hours in the oxidized state and the electroactive sites underwent ca. 440,000 turnovers.

The predicted chemistry in Rxn. 3 is coordination of pyridine groups in the polymer matrix to the $-IrCl_5^{2-}$ moiety, forming pendant ~ $PyIrCl_5^{2-}$ units. We have prepared unattached analog complexes by literature methods (22,23), and in 1 M H_2SO_4 the $Ir^{III/IV}$ reactions of $PyIrCl_5^{2-}$ and of (isonic)$IrCl_5^{2-}$ occur at respectively $E^{\circ\prime}_{soln}$ = +0.99 and +1.00 volt vs. S.C.E. $IrCl_6^{3-}$ itself reacts at +0.69 volt in 1 M HCl. Clearly, the +0.40 volt potential for the C/PPVPy ~ $IrCl_5^{2-}$ electrode wave in Figure 2 is not compatible with an $Ir^{III/IV}$ reaction in either of these coordination states. Potential excursions to +1.0 volt on C/PPVPy ~ $IrCl_5^{2-}$ electrodes

reveal no other more positive waves than that at +0.40 volt.

In the scheme of Rxns. 1-3 above, only the NO^+ ligand is expectably displaced and the form of the pendant iridium complex in the electrode is thus thought to be $\sim LIrCl_5^{2-}$. If the +0.40 volt wave for the iridium-metallated film is indeed due to an $Ir^{III/IV}$ reaction as opposed to reaction of a different redox site in the film (somehow activated by iridium coordination), then the very negative +0.40 volt redox potential (as compared to $IrCl_6^{3-}$ and $PyIrCl_5^{2-}$ and by analogy with the coordination properties of ruthenium complexes (24)) implies that the ligand coordinated to iridium is strongly electron donating. Elemental analysis of unmetallated plasma polymerized vinylpyridine indicates significant oxygen incorporation into the film, the empirical formula being $C_7H_{8.3}N_{1.0}O_{1.8}$ as compared to C_7H_7N ideally expected for polyvinylpyridine. The chemical nature of the oxygenated sites is unknown. It is unlikely that a hydroxylated pyridine coordinating the iridium would shift E° , as compared to unsubstituted pyridine, by 0.6 volt. The most likely basis for the +0.40 volt wave of Figure 2 would seem to be the $Ir^{III/IV}$ reaction of a $\sim ArO{-}IrCl_5^-$ complex, or a quinone-type moiety whose electron transfer chemistry is activated by iridium coordination.

In previous studies of plasma polymerized vinylferrocene films on electrodes, plasma damage and oxygen incorporation were noticed via elemental analyses and XPS (17,18), but the dominant chemical and electrochemical characteristics of the film remained those of the ferrocene group. The above results contrast with this; chemical damage effects associated with the vinylpyridine plasma polymerization are more profound and obscure understanding of the film's coordination chemistry. In the course of these studies, however, we discovered that the iridium metallated film is a potent catalyst for the

oxidation of ascorbic acid (vide infra) and so some additional characterization of the C/PPVPy ~ $IrCl_5^{2-}$ electrode properties was deemed worthwhile.

Charge Transport in C/PPVPy ~ $IrCl_5^{2-}$ Films. The coverage of electroactive centers measured from the Figure 2 surface wave is the equivalent of 25-30 monolayers of ~ $IrCl_5^{2-}$ groups (not accounting for surface roughness), and so the rate at which the electroactive centers in the film can become oxidized and reduced is of interest. On the cyclic voltammetric time scale, the rate at which electrochemical charge is transported through the film in 1 M H_2SO_4 is very fast, as shown by the linear proportionality measured between peak current, i_p, and potential scan rate, $\underline{v}$, from $\underline{v}$ = 0.02 to 5 v./s. This means that the ratio of oxidized and reduced sites in the film remains in Nernstian equilibrium with the electrode potential during the potential scan.

Given the Nernstian behavior, the number of electrons $\underline{n}$ transferred per electroactive site can be estimated from the i_p - $\underline{v}$ slope and the surface activity relationships for interacting sites (25)

$$i_p = n^2F^2A\Gamma_T\nu/RT[4-2r\Gamma_T] \qquad (4)$$

where the interaction parameter $r\Gamma_T$ = -0.28 is estimated from E_{FWHM} = 240 mv. using a working plot (26). This calculation gives n ~ 0.86 or a one electron reaction.

The current-time curve resulting from a -0.3 to +0.8 volt vs. SSCE potential step at a C/PPVPy ~ $IrCl_5^{2-}$ electrode in 1 M H_2SO_4 is shown in Figure 3, Curve A. On the short time scale achieved in this experiment, the rate of oxidative charging of the film controls the current-time decay. After subtracting background current as approximated with a -0.3 to +0.3

volt step (Curve B), Curve C shows a Cottrell plot of electroactive site oxidation current vs $t^{-1/2}$. At short times the plot is satisfactorily linear and demonstrates a diffusion controlled charge transport through the film where the concentration distance profile of oxidized and reduced sites in the film does not exceed the film thickness at short times. The charge transport rate can be obtained from the Cottrell equation as we have previously shown (18) for fixed site redox polymer films

$$i = nFAD_{ct}^{1/2} C/\pi^{1/2}t^{1/2} \qquad (5)$$

where C is the concentration of electroactive sites in the film. The data of Figure 3, Curve C, give $D_{ct}^{1/2}C = 5.8 \times 10^{-8}$ mol./cm.^{2}sec.$^{1/2}$. Assuming (27) a 300 nm film thickness, (i.e., C $\sim$ 0.2 M) gives $D_{ct} \sim 8 \times 10^{-8}$ cm.^{2}/sec. That the value of C and thus D_{ct} are approximate still leaves obvious the fact that D_{ct} in this film is as large or larger than other known charge transport diffusion constants (28,29).

At longer times in Figure 3, Curve C, the current falls below the Cottrell (dashed) line as expected (in fact required) when the concentration distance profiles intersect the film/solution boundary. At these times, finite diffusion theory applies (18), from which currents were calculated (—□—) in Figure 3 for $D_{ct}^{1/2}C = 5.8 \times 10^{-8}$. The theoretical currents fall slightly below the experimental ones (—○—) (Curve C) which could mean, among other things, that all sites in the film do not exhibit the same effective charge transport rate.

Electrolyte Effects. The cyclic voltammetry of C/PPVPy $\sim$ $IrCl_5^{2-}$ films is sensitive to the nature and concentration of the supporting electrolyte cation, but not the anion. Voltammetry in 1 M HCl and in 1 M $HClO_4$ is indistinguishable from that in Figure 2 except for a minor (10-20 mv.) potential

shift in $E^{o'}_{surf}$. Changing the supporting electrolyte cation, on the other hand, from H^+ to Li^+ (same as Cs^+) to Na^+ to K^+ to Bu_4N^+ produces the effects shown in Figure 4, broadening and attenuating the wave and shifting it to more negative potentials. Also, starting with 0.5 M Et_4NCl, in which the C/PPVPy ∿ $IrCl_5^{2-}$ wave is shifted and attenuated, Figure 5 shows that incrementally adding H^+ as HCl increases the quantity of reacting sites in the film and shifts the wave back to more positive potentials.

Attaching a molecular interpretation to these effects is difficult given the uncertainty in film composition. It may well be that the action of small electrolyte cations is to break up internal ion associations (e.g., electrostatic cross-linking) between anionic iridium sites and cationic sites like pyridinium, which otherwise impede charge transport (e.g., reduce the size of the wave) and shift $E^{o'}_{surf}$ negatively. Note in this connection that the order of the supporting electrolyte cation effects in Figure 4 is also the order of the hydrated ion sizes, including the similarity between Li^+ and Cs^+ .

Catalytic Oxidation With C/PPVP ∿ $IrCl_6^{2-}$ Films. The irreversible oxidation of ascorbic acid in 1 M H_2SO_4 on a naked carbon electrode occurs at $E_{p,a}$ = +0.76 volt vs. S.C.E. (Figure 6, Curve C) at an overpotential of 860 mv. compared to its thermodynamic potential of -0.1 volt. Ascorbic acid is also oxidized at +0.76 volt on a carbon electrode coated with (unmetallated) plasma polymerized vinylpyridine. The latter result means that o-quinone groups, known (30-32) to oxidize ascorbic acid, are probably not an important component of the polymer film, and also implies that the film is sufficiently solvent swollen that ascorbic acid can diffuse through it to undergo electron transfer at the carbon/film interface.

That ascorbic acid gains access to the carbon/film interface by diffusion through the film rather than through pinholes in the film (33) can be

inferred from rotated disk electrode voltammetry. Voltammograms of ascorbic acid at rotated electrodes bearing unmetallated films (Figure 7, Curve B) were determined as a function of electrode rotation rate, ω. In contrast to those at naked carbon (which occur at the same potential) the Levich $i_{lim} - \omega^{1/2}$ plots for voltammograms at film covered electrodes are non-linear as shown in Figure 8, Curve B. This non-linearity is consistent with partial control of current by the rate of diffusion through a membrane, the appropriate relationship (34) for which is

$$\frac{1}{i_{lim}} = \frac{1}{nFAD_{S,pol}PC_S/d} + \frac{1}{0.62nFAD_S^{2/3}\nu^{-1/6}\omega^{1/2}C_S} \qquad (6)$$

where $D_{S,pol}$ and P are the diffusion and partition coefficients for ascorbic acid in the film, respectively, C_S is its solution concentration, and the right hand term is the Levich relation. The inset in Figure 8 shows the data from Curve B plotted according to equation 6; the linear relation is evident. Extrapolation to $1/\omega^{1/2} = 0$ gives from the intercept a flux $D_{S,pol}PC_S/d = 1 \times 10^{-8}$ mol./cm.^{2}sec. in the film. Approximating film thickness as 300 nm as above (27), and assuming P = 1, gives $D_{S,pol} = 4 \times 10^{-7}$ cm.^{2}/sec. This value is only about an order of magnitude smaller than that for ascorbic acid diffusing in solution (35), $D_S = 5.7 \times 10^{-6}$ cm.^{2}/sec., indicating that the unmetallated film has a fairly open structure.

When the film is metallated with iridium, oxidation of ascorbic acid on the C/PPVPy $\sim$ $IrCl_5^{2-}$ electrode becomes in cyclic voltammetry, voltage catalyzed by about 230 mv. as shown by Figure 6, Curve B. The electrocatalytic oxidation is rapid and, by the criterion of proportionality of the peak current, $i_{p,a}$, to $\nu^{1/2}$ (ν = potential scan rate, Figure 9), controlled by diffusion of ascorbic acid to the electrode. The slope of Figure 9 agrees

within a factor of 1.4 with that calculated from the irreversible potential sweep relation (36) using the known diffusion coefficient for ascorbic acid (25) and $\alpha = 0.5$.

The electrocatalytic oxidation of ascorbic acid by rotated disk C/PPVPy ~ $IrCl_5^{2-}$ electrode voltammetry gives voltammograms like Figure 7, Curve C. The voltage catalysis is not as striking as in cyclic voltammetry, but is clearly evident. The limiting current for Curve C is greater than that for the unmetallated film (Curve B). A plot of i_{lim} *vs.* $\omega^{1/2}$ for Curve C (shown in Figure 8, Curve C) shows that within the limits of experimental error the currents follow the Levich equation. Thus, in the EC catalysis equation (7)

$$\frac{1}{i_{lim}} = \frac{1}{nFAk_{ch}\Gamma C_S} + \frac{1}{0.62nFAD_S^{2/3}\nu^{-1/6}\omega^{1/2}C_S} \qquad (7)$$

the maximum attained Levich (solution mass transport) flux 2×10^{-8} mol./cm.^{2} sec. remains less than that allowed by the catalytic reaction $k_{ch}\Gamma C_S$ for the consumption of ascorbic acid. We estimate from this result that the effective heterogeneous rate constant for ascorbic acid at the C/PPVPy ~ $IrCl_6^{2-}$ surface, $k_{ch}\Gamma$, must exceed 0.1 cm./sec. From this, the rate constant for reaction between ascorbic acid and oxidized catalyst sites is $k_{ch} > 5 \times 10^5$ $M^{-1}sec^{-1}$ or $> 2 \times 10^4$ $M^{-1}sec^{-1}$ depending on whether one assumes that only the outermost monomolecular layer ($\Gamma \sim 2 \times 10^{-10}$ mol./cm.^{2}) is active in the reaction, or that all of the catalyst sites in the film ($\Gamma = \Gamma_T = 5 \times 10^{-9}$ mol./cm.^{2}). This is among the fastest modified electrode catalytic rates known (1,2,4,10,11).

The phenomenon of membrane limited diffusion (Figure 8 inset) is not seen in the C/PPVPy ~ $IrCl_5^{2-}$ catalyzed electrochemistry, which further demonstrates that the locus of ascorbic acid oxidation is now catalytic sites in

the film rather than the carbon/film interface. It is not plausible that the metallation reaction has in addition to a catalytic effect rendered the film even more permeable to ascorbic acid (e.g., that $D_{S,pol}P$ should increase). The metallated film in fact is now poorly permeable; the cyclic voltammetry of methylviologen in 1 M H_2SO_4 is completely suppressed on C/PPVpy ∿ $IrCl_5^{2-}$ electrodes. Methyl viologen reacts at a potential inappropriate for electrocatalysis by redox sites in the film so in order to react, it is obligated to diffuse through the film to the carbon/film interface.

Finally, the ordering of rate processes (excluding the Levich mass transport) can be estimated in the following way. As noted above, the flux due to the chemical consumption of ascorbic acid exceeds 1×10^{-7} mol./cm.^{2}sec. From the charge transport rate measurement, the effective steady state flux of electrochemical charge through the film cannot exceed $(D_{ct}^{1/2}C)^2/\Gamma_T = D_{ct}\, C/d \sim 6 \times 10^{-7}$ mol./cm.^{2}sec. Lastly, the flux of ascorbic acid diffusing entirely through the film is as an upper boundary, 1×10^{-8} mol./cm.^{2}sec. (vide supra, Figure 8). From this comparison, it is clear that the available chemical and charge transport fluxes both exceed the flux capability for ascorbic acid diffusion in the film and so the reaction zone for the electrocatalytic process must be localized to a few layers of catalyst sites at the film/solution boundary. We have previously discussed flux comparisons of this sort (9,15,16).

In preliminary experiments, we have ascertained that the C/PPVPy ∿ $IrCl_5^{2-}$ electrode also catalyzes oxidation of dopamine and similar substrates, but the extent of voltage catalysis is variable and differs from that for ascorbic acid. Figure 10 shows that at naked carbon (Curve A), dopamine and ascorbic acid are oxidized at identical potentials, but on a C/PPVpy ∿ $IrCl_5^{2-}$ electrode, $E_{p,a}$ for oxidation of the two substrates occurs at different potentials (Curves B,C). Resolution of the voltammetric waves of dopamine

and ascorbic acid is of interest relative to neurochemical and analytical studies (32,37,38). The voltage resolution in Figure 10 is analytically useful. It would, nevertheless, be more desirable analytically that dopamine be more strongly catalyzed than ascorbic acid (the reverse of Figure 10).

Lastly, we call attention to the anomalous difference between the oxidation potentials of dopamine and ascorbic acid and for the redox sites in the iridium metallated film. In an uncomplicated EC electrocatalytic reaction mechanism, the dopamine and ascorbic acid reactions should occur at potentials close to that for the ostensible catalyst wave. Again, uncertainty in the chemical makeup of the film obviates a molecular interpretation of this problem. We should note that one way the film could remain inactive until nearly all of the catalyst sites become oxidized would be a reactivity strongly dependent on the degree of electrostatic cross-linking within the film. Oxidation of the anionic catalyst sites would relieve the electrostatic interactions by lowering the charge on those sites.

Acknowledgement. This research was supported in part by a grant from the Office of Naval Research. Helpful discussions with B. P. Sullivan are gratefully acknowledged.

REFERENCES

1. Murray, R. W. Acc. Chem. Res. 1980, 13, 135.
2. Oyama, N.; Anson, F. C. Anal. Chem. 1980, 52, 1192.
3. Shigehara, K.; Oyama, N.; Anson, F. C. Inorg. Chem., 1981, 20, 518.
4. Collman, J. P.; Denisevich, P.; Konai, Y.; Marrocco, M.; Koval, C.; Anson, F. C. J. Amer. Chem. Soc. 1980, 102, 6027.
5. Bettelheim, A.; Chan, R. J. H.; Kuwana, T. J. Electroanal. Chem., 1980 110, 93.
6. Degrand, C.; Miller, L. L. J. Amer. Chem. Soc. 1980, 102, 5728.
7. Calvert, J. M.; Meyer, T. J. Inorg. Chem. 1981, 20, 27.
8. Abruña, H. D.; Walsh, J. L.; Meyer, T. J.; Murray, R. W. J. Amer. Chem. Soc. 1980, 102, 3272.
9. Rocklin, R. D.; Murray, R. W. J. Phys. Chem., in press.
10. Ikeda, T.; Leidner, C. R.; Murray, R. W. J. Amer. Chem. Soc., submitted.
11. Lewis, N. S.; Bocarsly, A. B.; Wrighton, M. S. J. Phys. Chem. 1980, 84, 2033.
12. Andrieux, C. P.; Saveant, J. M. J. Electroanal. Chem. 1978, 93, 163.
13. Andrieux, C. P.; Dumas-Bouchiat, J. M.; Saveant, J. M. J. Electroanal. Chem. 1980, 114, 159.
14. Anson, F. C. J. Phys. Chem. 1980, 84, 3336.
15. Daum, P.; Murray, R. W. J. Phys. Chem. 1981, 85, 389.
16. Murray, R. W. Philos. Trans. Royal Soc. (London), in press.
17. Nowak, R. J.; Schultz, F. A.; Umaña, M.; Lam, R.; Murray, R. W. Anal. Chem. 1980, 52, 315.
18. Daum, P.; Lenhard, J. R.; Rolison, D.; Murray, R. W. J. Amer. Chem. Soc. 1980, 102, 4649.

19. Facci, J. University of North Carolina, 1980, unpublished results.

20. Oyama, N.; Anson, F. C. J. Amer. Chem. Soc. 1979, 101, 739.

21. Martin, G. W., Ph.D. Thesis, University of North Carolina, 1977.

22. Bottomley, F.; Clarkson, S. G.; Tong, S. J. Chem. Soc. Dalton 1974, 2344.

23. Delepine, M. Comptes Rendues 1911, 152, 1390, 1589.

24. Salmon, D., Ph.D. Thesis, University of North Carolina, 1977.

25. Brown, A. P.; Anson, F. C. Anal. Chem. 1977, 49, 1589.

26. Smith, D. F.; Willman, K.; Kuo, K.; Murray, R. W. J. Electroanal. Chem. 1979, 95, 217.

27. The electrodes are blue in color. Assuming reflective interference occurs, the equation $2d = (n+1/2)\lambda$ applies. When n = 0, 1, 2, d, the thickness of the coating can be 100, 300, or 500 nm. We are assuming the median value.

28. Peerce, P. J.; Bard, A. J. J. Electroanal. Chem. 1980, 114, 89.

29. Nakahama, S. University of North Carolina, 1980, unpublished results.

30. Evans, J. F.; Kuwana, T.; Henne, M. T.; Royer, G. P. J. Electroanal. Chem. 1977, 80, 409.

31. Bettleheim, A.; Chan, R. J. H.; Kuwana, T. J. Electroanal. Chem. 1979, 99, 391.

32. Cheng, H.-Y.; Strope, E.; Adams, R. N. Anal. Chem. 1979, 51, 2243.

33. Peerce, P. J.; Bard, A. J. J. Electroanal. Chem. 1980, 112, 97.

34. Gough, D. A.; Leypoldt, J. K. Anal. Chem. 1979, 51, 439.

35. Kolthoff, I. M.; Ligane, J. J. "Polarography", Vol. 2; Interscience: New York, 1952; p. 729.

36. Bard, A. J.; Faulkner, L. R. "Electrochemical Methods", Wiley: New York, 1980; p. 222.

37. Lane, R. F.; Hubbard, A. T. Anal. Chem. 1976, 48, 1287.

38. Adams, R. N. Anal. Chem. 1976, 48, 1126A.

FIGURE LEGENDS

Figure 1. Schematic of electrode holder (glass flute) used in plasma polymerization of 4-vinylpyridine. Side and front view. Wells 1-3 contain electrodes, well 4 contains 10-20 μl. VPy.

Figure 2. Cyclic voltammetry of C/PPVPy ~ $IrCl_5^{2-}$ film in 1 M H_2SO_4 at 0.1 v./s. $Q_{ox} = Q_{red}$. S = 150 μa./cm.^{2}. $\Gamma = 5.7 \times 10^{-9}$ mol./cm.^{2} .

Figure 3. Chronoamperometric current-time response (Curve A), background current (Curve B), and plot of corrected current vs. $t^{-1/2}$ (Curve C) for C/PPVPy ~ $IrCl_5^{2-}$ in 1 M H_2SO_4 . Slope of Curve C = 0.223 A.sec.$^{1/2}$ which gives $D_{ct}{}^{1/2}C = 5.8 \times 10^{-8}$ mol./cm.^{2}sec.$^{1/2}$. Circles are experimental points, squares are currents calculated from $D_{ct}{}^{1/2}C = 5.8 \times 10^{-8}$ and eq. 5 of ref. 18.

Figure 4. Effect of electrolyte cation in cyclic voltammetry of C/PPVPy ~ $IrCl_5^{2-}$. Aqueous solutions 1 M $HClO_4$ (Curve A), 1 M $LiClO_4$ or 0.1 M $CsClO_4$ (Curve B), 1 M $NaClO_4$ (Curve C), 1 M KCl or 1 M Et_4NCl (Curve D), and 1 M Bu_4NBr (Curve E), 0.2 v./s., S = 300 μa./cm.^{2} .

Figure 5. Effect of $[H^+]$ on C/PPVPy ~ $IrCl_5^{2-}$ cyclic voltammetry. 0.5 M HCl (Curve A), 0.5 M Et_4NCl + 0.1 M HCl (Curve B), 0.5 M Et_4NCl + 0.01 M HCl (Curve C), 0.5 M Et_4NCl + 0.001 M HCl (Curve D), 0.5 M Et_4NCl (Curve E), 0.2 v./s., 300 μa./cm.^{2}

Figure 6. Electrocatalytic oxidation of ascorbic acid in 1 M H_2SO_4 . Curve A: C/PPVPy ∿ $IrCl_5^{2-}$ electrode alone, S = 140 μa./cm.^{2}; Curve B: C/PPVPy ∿ $IrCl_5^{2-}$ with 10 mM ascorbic acid, S = 700 μa./cm.^{2}; Curve C: 10 mM ascorbic acid at naked glassy carbon, S = 700 μa./cm.^{2}; 0.1 v./s.

Figure 7. Rotated disk electrode voltammetry at 3600 rpm in 1 M H_2SO_4 of (Curve A) C/PPVPy ∿ $IrCl_5^{2-}$ electrode, (Curve B) unmetallated C/PPVPy electrode in 1 mM ascorbic acid, and (Curve C) C/PPVPy ∿ $IrCl_5^{2-}$ electrode in 1 mM ascorbic acid. S = 140 (Curve A) and 700 (Curves B,C) μa./cm.^{2}

Figure 8. Levich plots for limiting currents for oxidation of 1 mM ascorbic acid on (Curve A) naked glassy carbon, (Curve B) unmetallated C/PPVPy electrode, and (Curve C) C/PPVPy ∿ $IrCl_5^{2-}$ electrode. Inset is plot of equation 6 for data of Curve B. All in 1 M H_2SO_4.

Figure 9. Relationship of potential sweep rate and peak current for Curve B of Figure 6.

Figure 10. Curve A: oxidation of a mixture of ascorbic acid and dopamine at naked glassy carbon , S = 1.4 ma./cm.^{2}, v = 0.2 v./s.; Curve B: oxidation of dopamine at C/PPVPy ∿ $IrCl_5^{2-}$, S = 280 μa./cm.^{2}, v = 0.1 v./s.; Curve C: oxidation of ascorbic acid at C/PPVPy∿$IrCl_5^{2-}$, S = 280 μa./cm.^{2}, v = 0.1 v./s. All in 1 M H_2SO_4 .

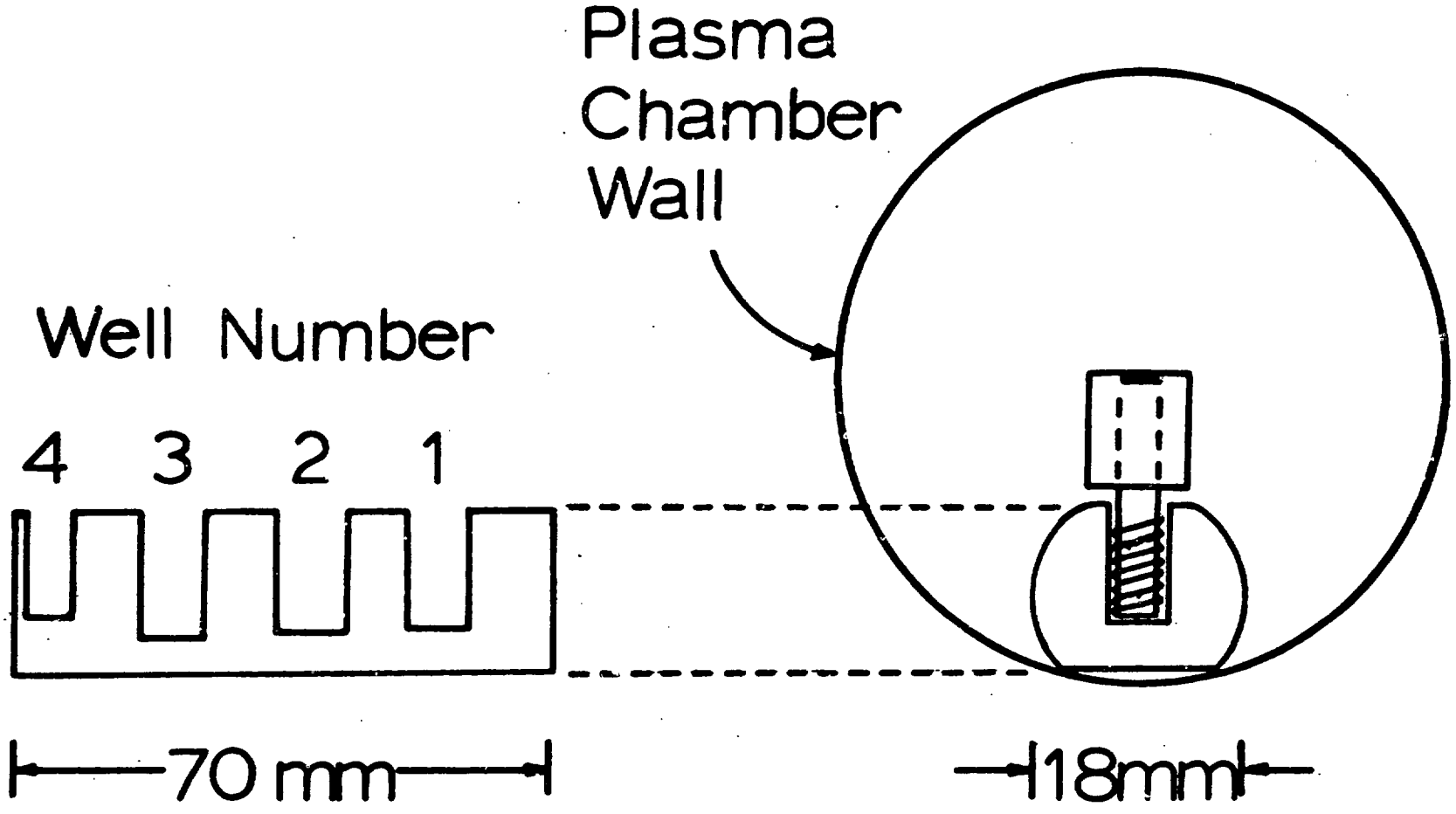
Plasma
Chamber
Wall
Well Number
4 3 2 1
70 mm
18mm

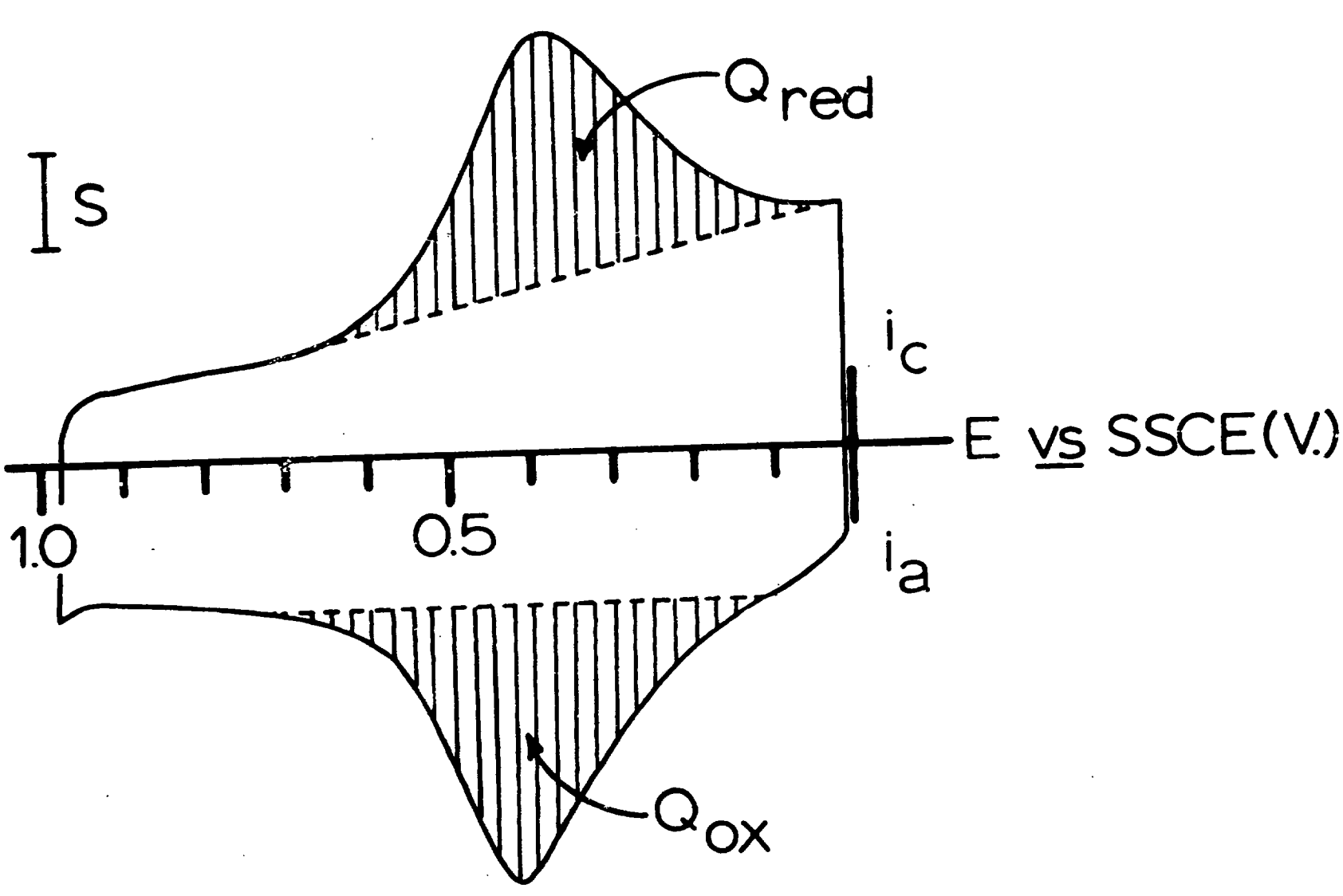
Is
Q red
i c
E vs SSCE(V.)
1.0
0.5
i a
Q ox

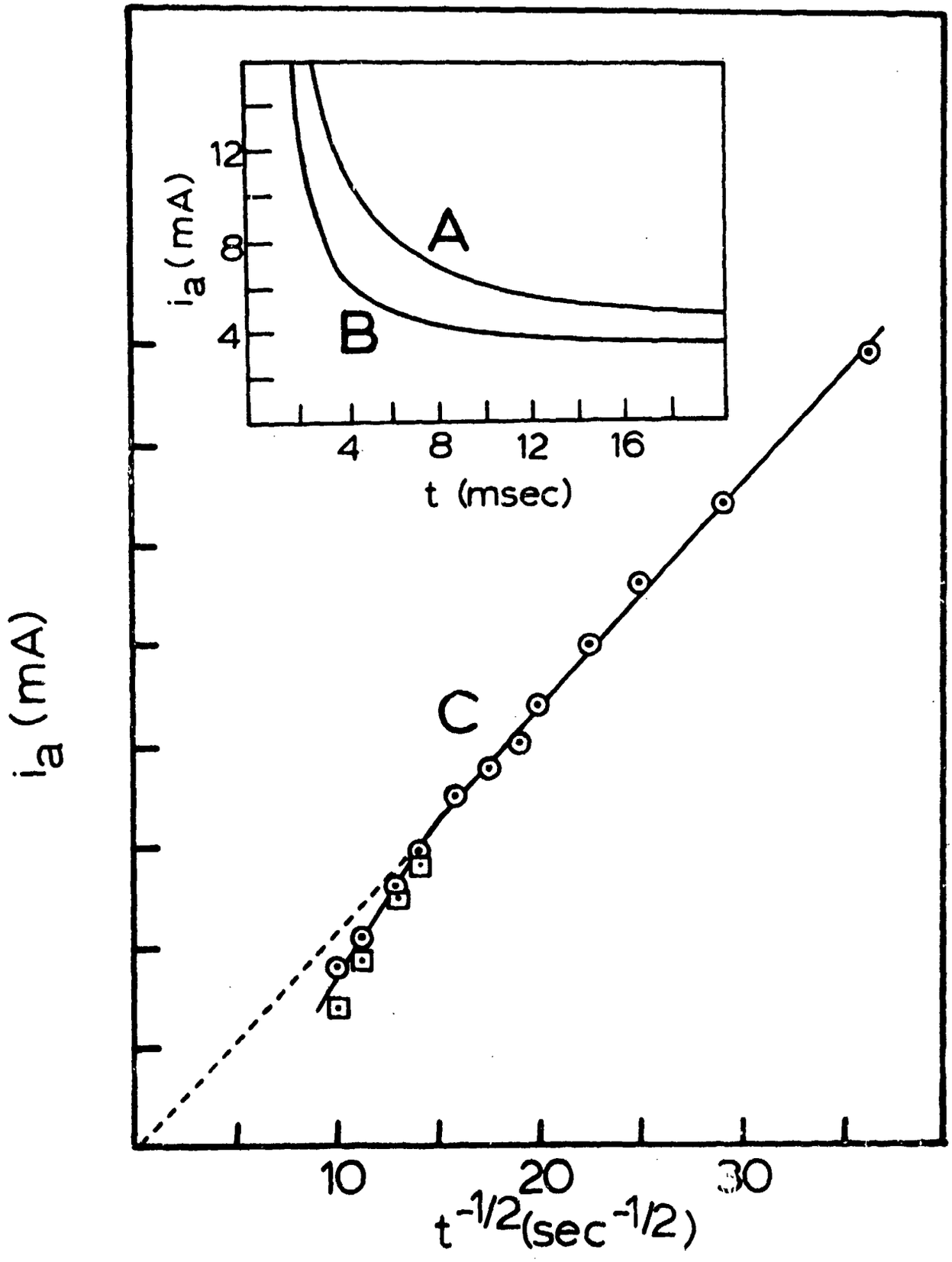
12
8
4
i_a (mA)
A
B
4
8
12
16
t (msec)
i_a (mA)
C
10
20
30
$t^{-1/2}$ (sec$^{-1/2}$)

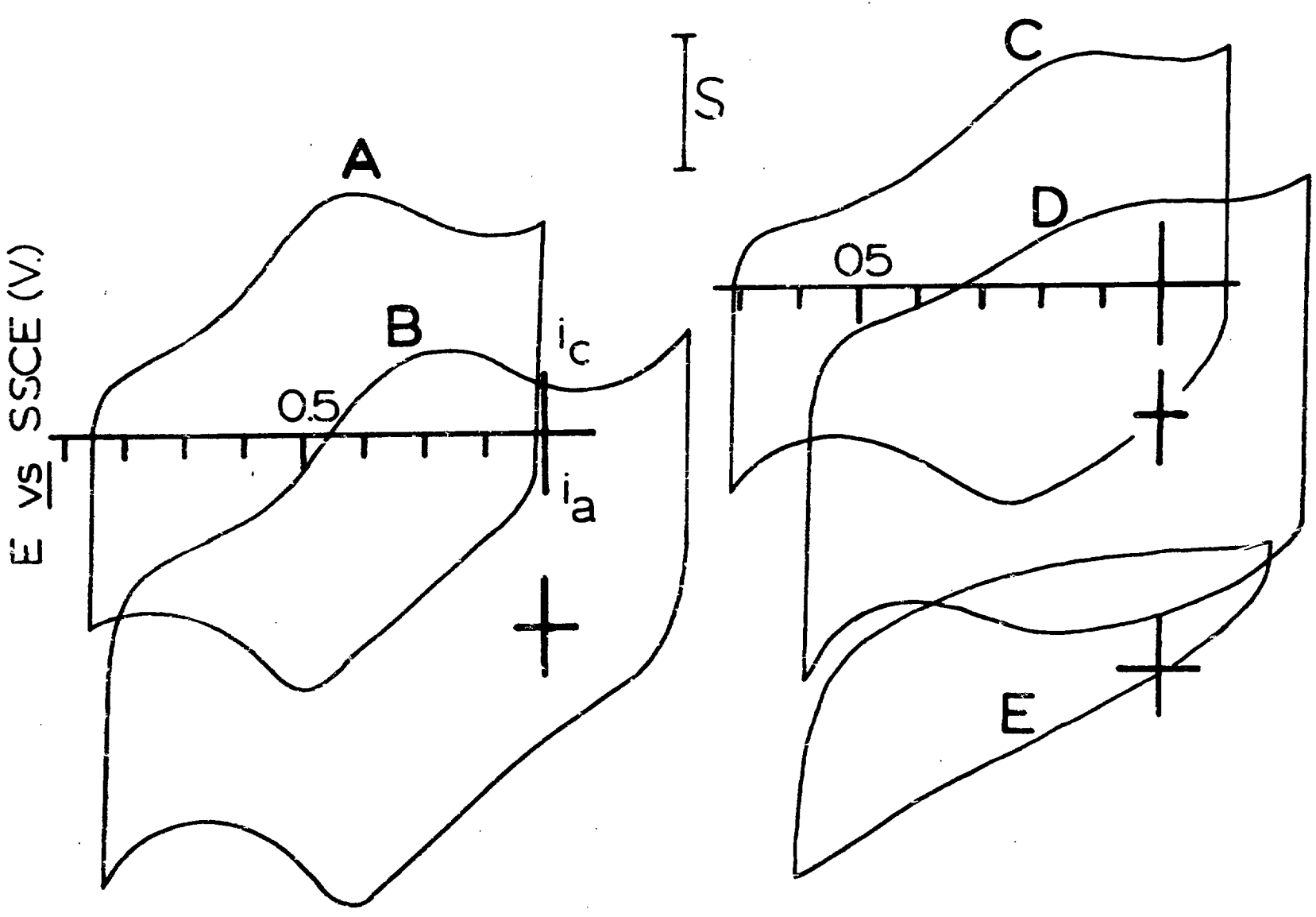
A
B
C
D
E
S
0.5
0.5
i_c
i_a
E vs SSCE (V.)

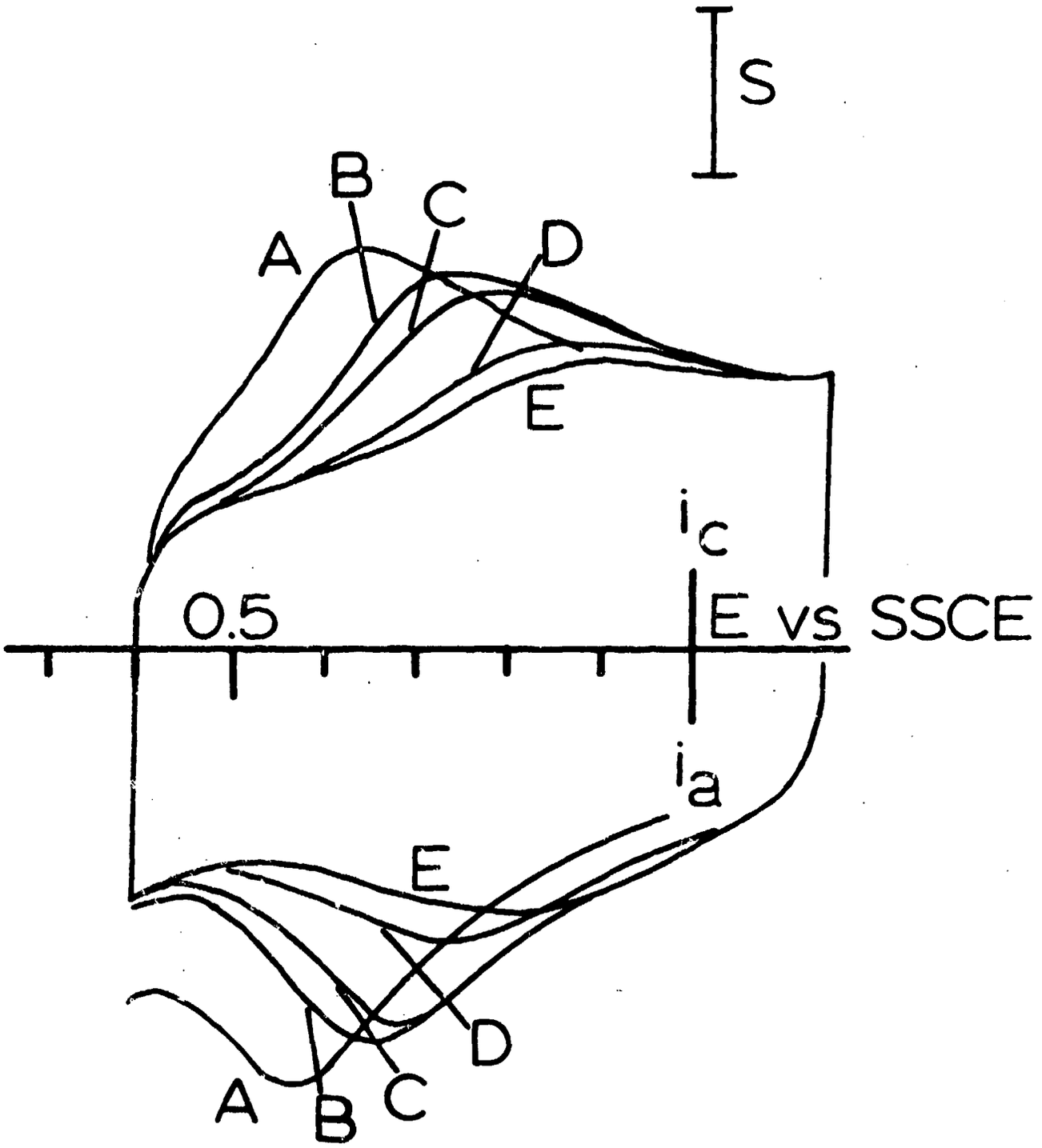
S
B
C
A
D
E
i_c
0.5
E vs SSCE
i_a
E
D
A
B
C

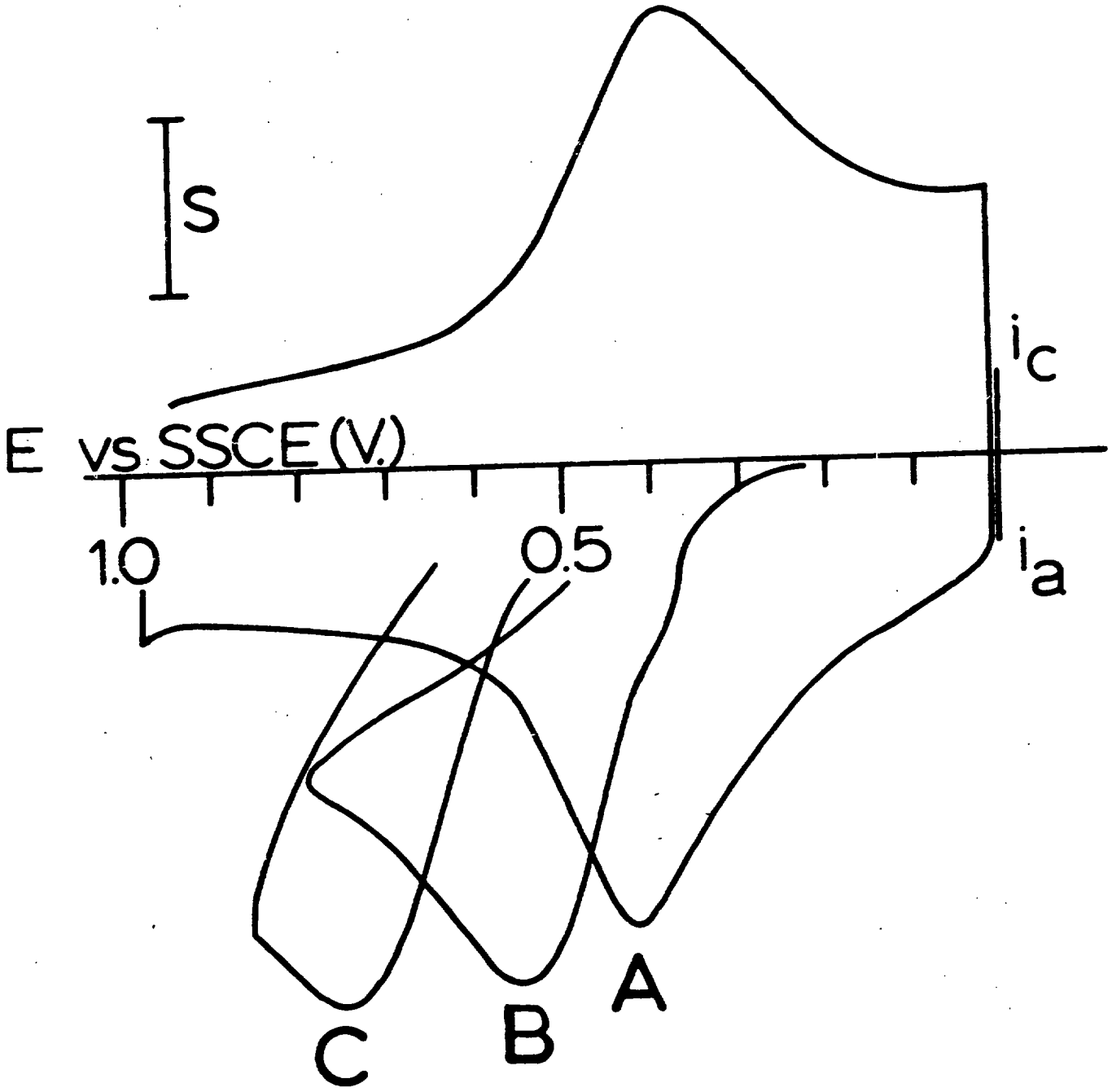
S
i_c
E vs SSCE (V.)
1.0
0.5
i_a
C
B
A

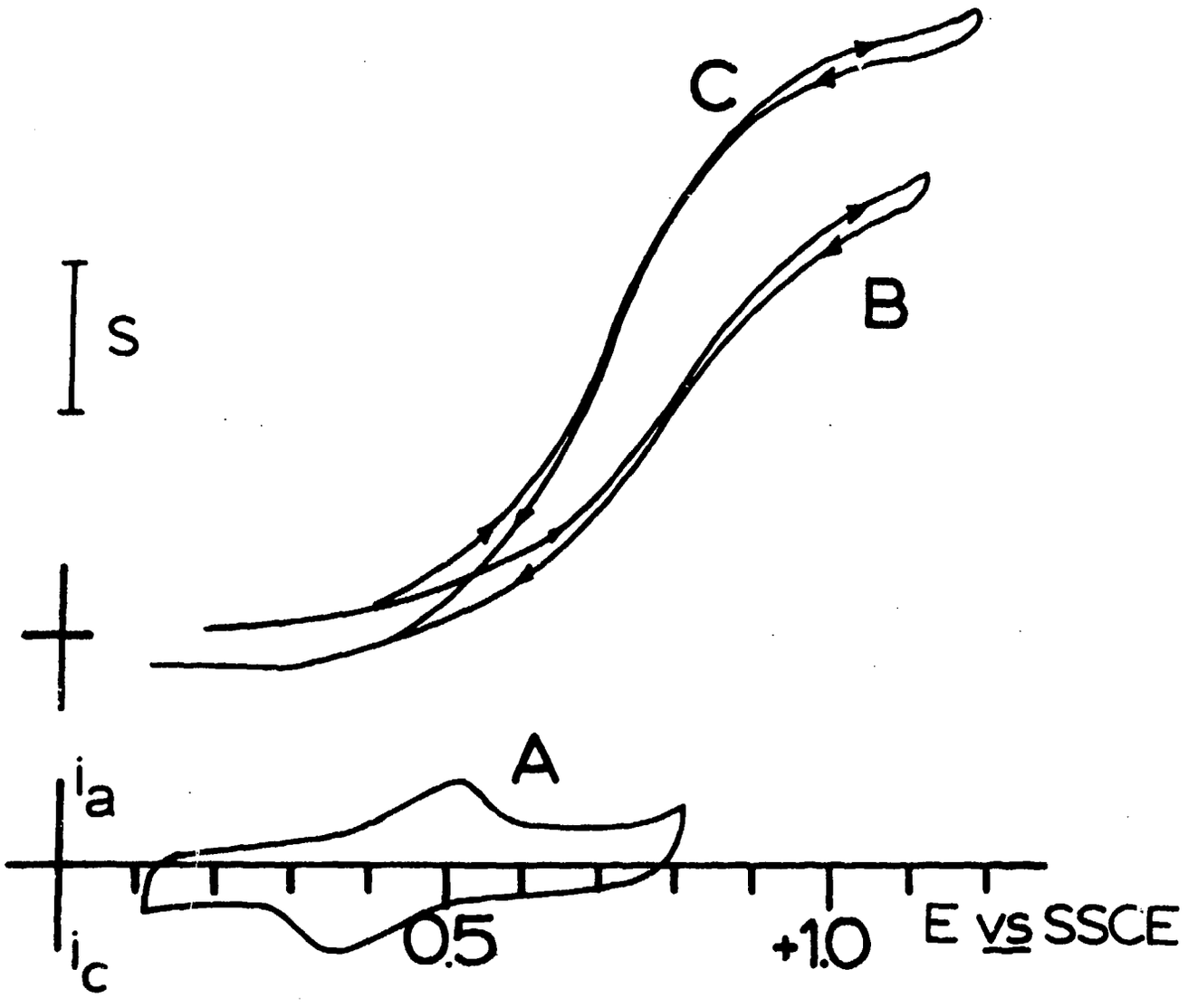
C
B
S
A
i_a
i_c
0.5
+1.0
E vs SSCE

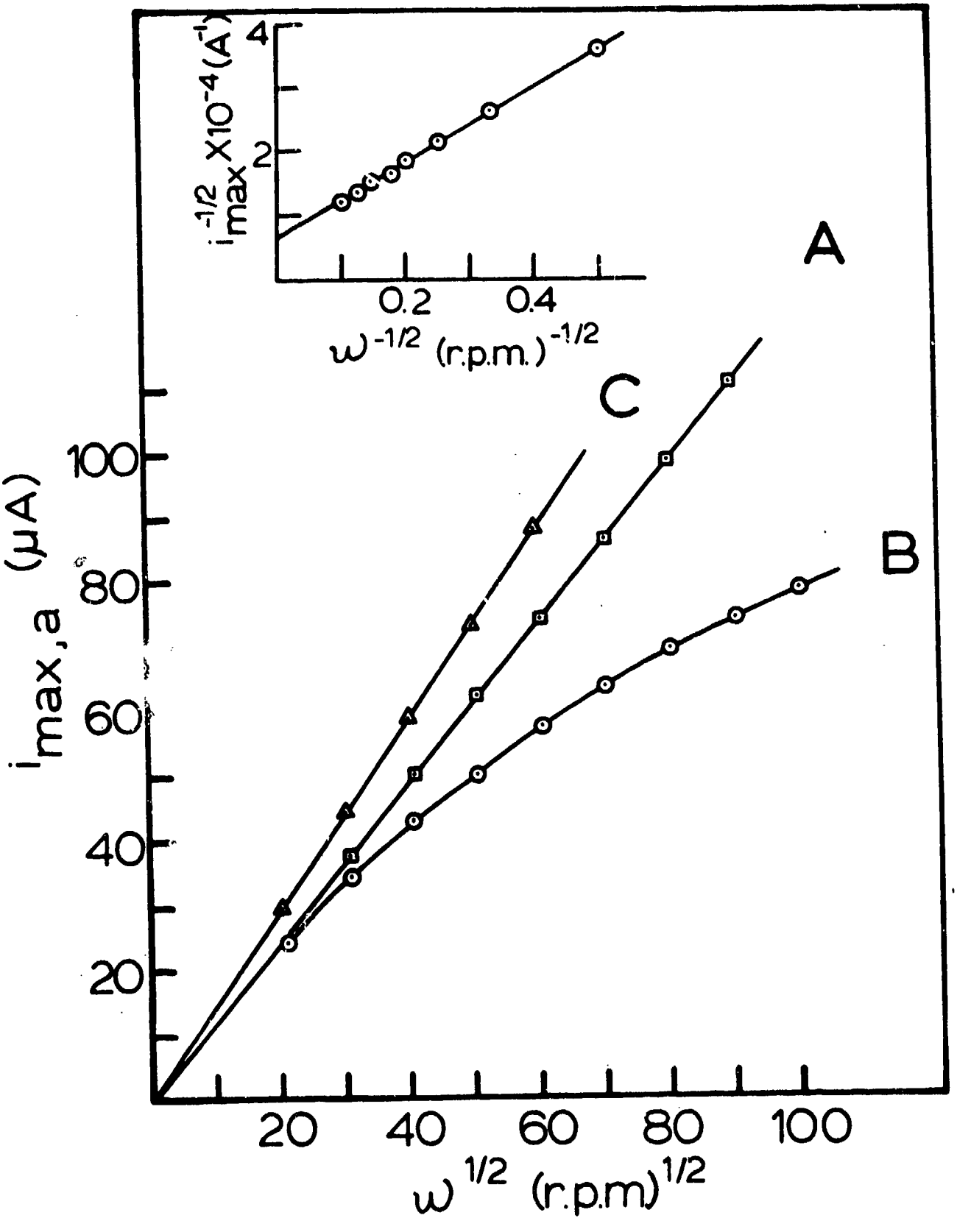
$i_{max}^{-1/2} X10^{-4} (A^{-1})$
4
2
0.2
0.4
$\omega^{-1/2}$ (r.p.m.)$^{-1/2}$
A
C
B
$i_{max,a}$ (μA)
100
80
60
40
20
20
40
60
80
100
$\omega^{1/2}$ (r.p.m)$^{1/2}$

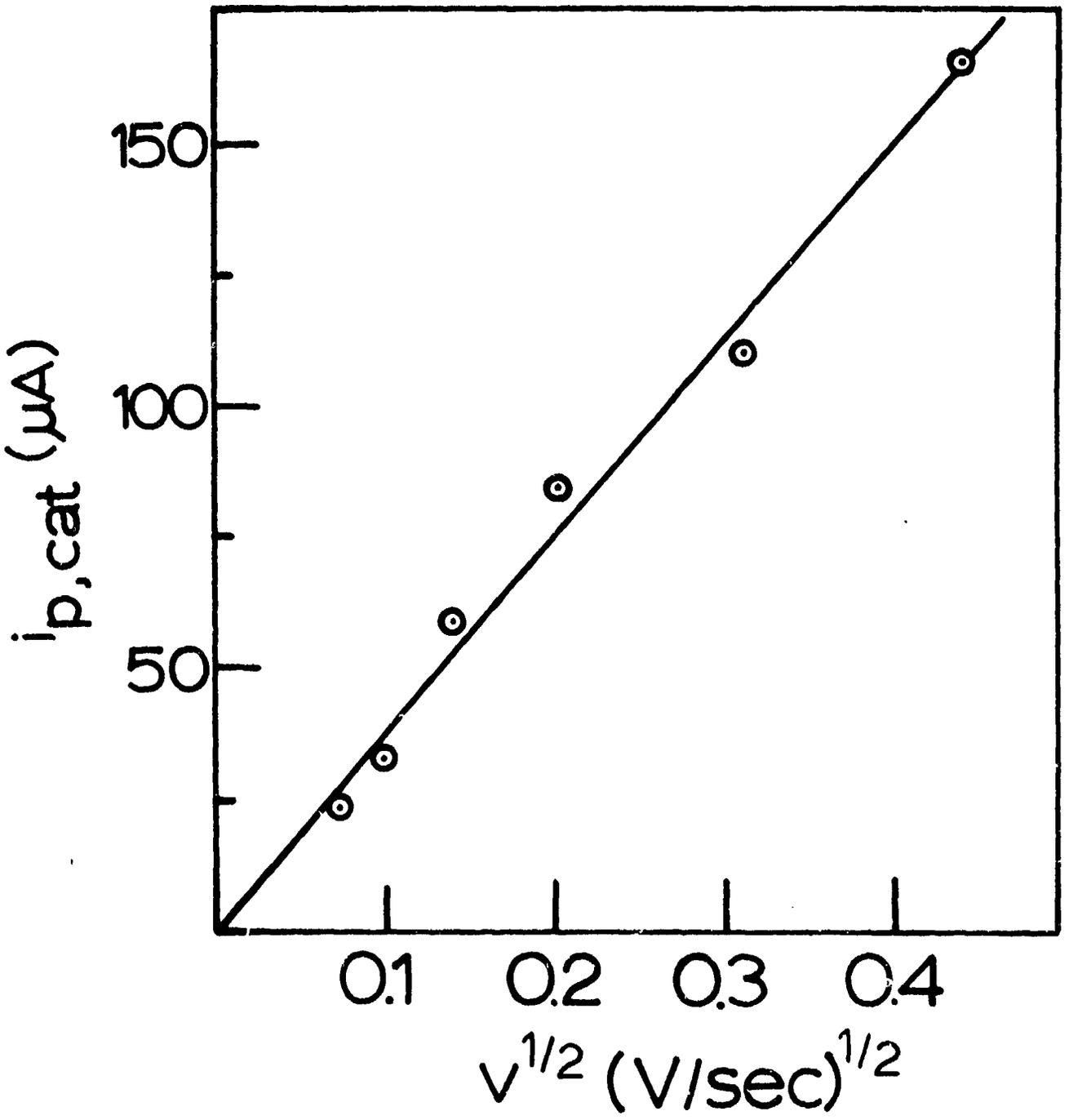
150
100
50
$i_{p,cat}$ (μA)
0.1
0.2
0.3
0.4
$v^{1/2}$ (V/sec)$^{1/2}$

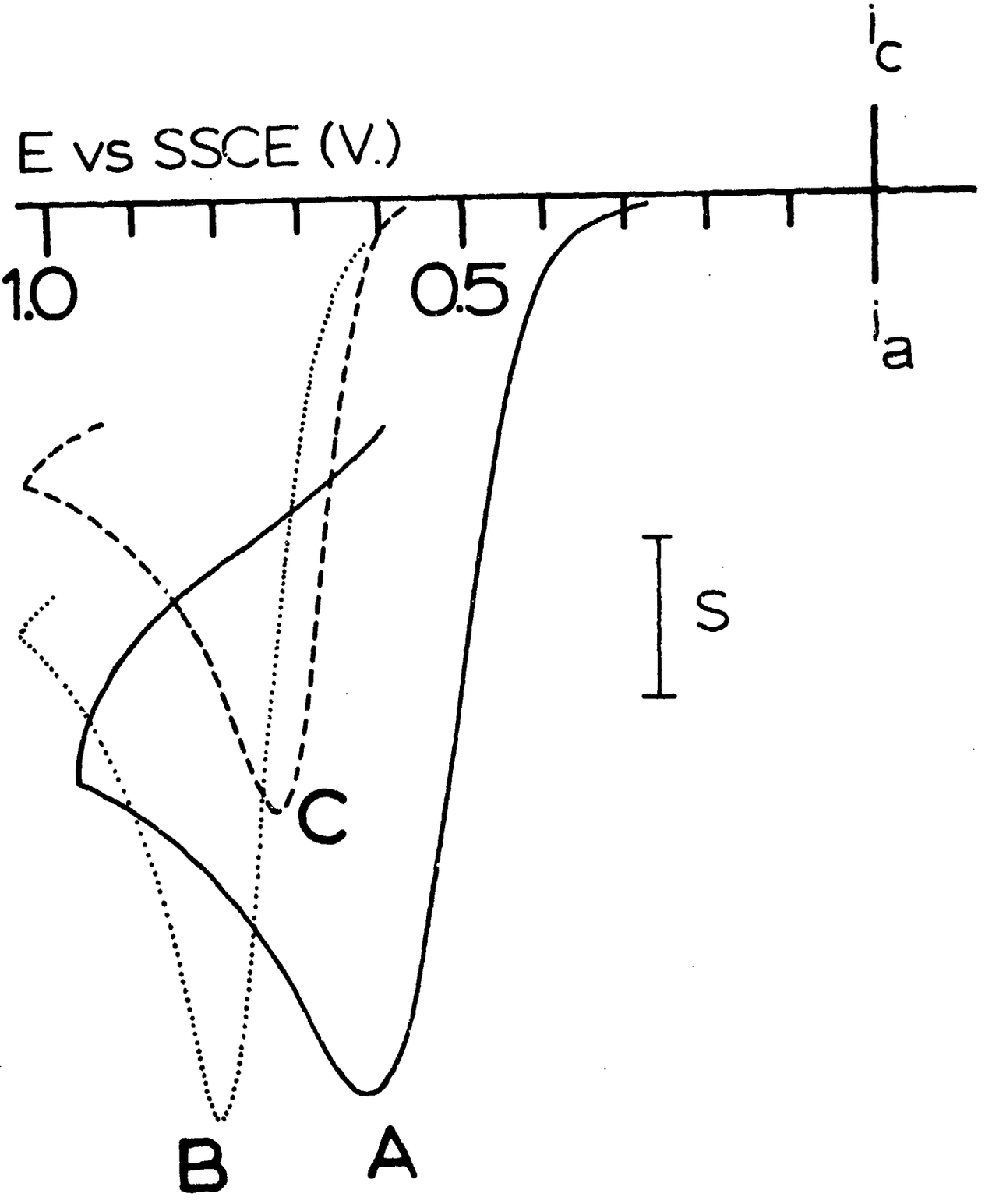
E vs SSCE (V.)
1.0
0.5
i_c
i_a
S
C
B
A